Available online at www.sciencedirect.com

ScienceDirect

Procedia Engineering 98 (2014) 20 – 27

Procedia Engineering

www.elsevier.com/locate/procedia

11th International Symposium on Systems with Fast Ionic Transport, ISSFIT 11

Optimization of sulphur content in $LiMn_2O_{4-y}S_y$ spinels as cathode materials for lithium-ion batteries

M. Bakierska[a], M. Molenda[a]*, R. Dziembaj[a,b]

[a] *Jagiellonian University, Faculty of Chemistry, Ingardena 3, 30-060 Krakow, Poland*
[b] *State Higher Vocational School, Mickiewicza 8, 33-100 Tarnow, Poland*

Abstract

Sulphur doped lithium manganese spinels with a nominal composition of $LiMn_2O_{4-y}S_y$ ($0 \leq y \leq 0.02$) were synthesized by a modified sol-gel method followed by calcinations at 300 and 650 °C in air. The prepared materials were characterized in terms of physicochemical properties using X-ray powder diffraction (XRD), differential scanning calorimetry (DSC) and electrical conductivity studies (EC). Electrochemical characteristic of $Li/Li^+/LiMn_2O_{4-y}S_y$ cells was examined by galvanostatic charge/discharge tests (CELL TEST), cyclic voltammetry (CV) and electrochemical impedance spectroscopy (EIS). It was shown that small amount of sulphur in $LiMn_2O_4$ spinel enhances the structural integrity of the host material and increases the electrochemical performance.

Peer-review under responsibility of the Gdansk University of Technology

Keywords: Li-ion batteries; cathode material; $LiMn_2O_4$; sulphided lithium manganese spinel; sol-gel

1. Introduction

Among the well known cathode materials for high power lithium-ion batteries, needed for electric vehicles (EV) and for renewable energy storage systems, the lithium manganese oxide spinels are still taken into account as one of the most promising candidates [1-3]. The $LiMn_2O_4$ spinel is very attractive in many aspects, such as high thermal and chemical stability, good safety, low toxicity, natural abundance, low cost and similar practical capacity (about

* Corresponding author. Tel.: +48-12-663-22-80; fax: +48-12-634-05-15.
E-mail address: molendam@chemia.uj.edu.pl

Peer-review under responsibility of the Gdansk University of Technology
doi:10.1016/j.proeng.2014.12.482

140 $mAhg^{-1}$), compared to commonly used materials – layered cobalt oxide $LiCoO_2$ and related systems, which suffer from the high toxicity and limited availability of cobalt sources [4-6]. Despite these advantages, practical application of Li-Mn-O materials is restricted, due to their structural instability. Close to room temperature $LiMn_2O_4$ spinel undergoes a reversible phase transition that causes capacity fading upon cycling and which is generally attributed to the Jahn-Teller distortion [7,8].

The structural stabilization of lithium manganese spinel and consequently, effective improvement of its electrochemical performance is a challenging issue and can be achieved by various strategies [9-12]. The izoelectronic partial substitution of sulphur in the oxygen sublattice of stoichiometric spinel is among them [13,14].

In the present work, nanosized stoichiometric $LiMn_2O_4$ and nonstoichiometric $LiMn_2O_{3.99}S_{0.01}$, $LiMn_2O_{3.98}S_{0.02}$ spinels were synthesized by the modified sol-gel method [15]. The obtained $LiMn_2O_{4-y}S_y$ samples were characterized in terms of sulphur substitution effect on their physico- and electrochemical properties. During this study optimal content of sulphur in the Li-Mn-O-S systems was established.

2. Experimental

A set of Li-Mn-O-S spinels was synthesized by the modified sol-gel method. For the preparation process, aqueous solutions of $CH_3COOLi{\cdot}2H_2O$, $(CH_3COO)_2Mn{\cdot}4H_2O$, $(NH_4)_2S$ and $NH_3{\cdot}H_2O$ as the alkalizing agent were used. Each of the synthesis was performed under constant flow of argon to avert oxidation of the Mn^{2+} ions. Condensation of the formed soles was accomplished at 90 °C for 3 ÷ 4 days under ambient pressure. After that, the obtained xerogels were calcined in air at 300 °C for 24 h with a heating rate equal to 1 $°Cmin^{-1}$, followed by additional high-temperature calcination at 650 °C for 6 h with a heating rate 5$°Cmin^{-1}$.

To determine the crystal structure of the resulting materials X-ray diffraction (XRD) measurements were carried out on BRUKER D2 PHASER with Cu K_α radiation (λ = 0.154184 nm) in the range of 10 ÷ 80 ° (2θ). The phase analysis of the XRD patterns was performed according to ICDD standards. The mean size of nanocrystallites was calculated from the full width at half maximum of (111) peak of the cubic spinel using Scherrer formula.

Differential scanning calorimetry (DSC) experiments were also conducted on the synthesized spinels. The data were collected using a Mettler Toledo 821^e microcalorimeter equipped with intracooler Haake at a scan rate of 10 $°Cmin^{-1}$ over the temperature range of -20 ÷ 50 °C.

The electrical conductivity of obtained samples was measured using the four-probe AC method at 33 Hz within temperature range of -20 ÷ 40 °C.

The electrochemical tests of the synthesized powders were carried out using 2032 coin cells. $Li/Li^+/LiMn_2O_{4-y}S_y$ ($0 \le y \le 0.02$) cells were assembled in a glove box under argon with both H_2O and O_2 levels less than 0.1 ppm. The electrolyte was a 1M solution of $LiPF_6$ in a mixture of EC, DEC (1:1). Positive electrodes were fabricated with 90 wt% of $LiMn_2O_{4-y}S_y$ spinel and 10 wt% of carbon black and placed on an aluminum crucible without using any binder. Loading of active material (Li-Mn-O-S system) in the assembled cells was about 9.2 mg. As a negative electrode, a lithium foil was used. Both electrodes were separated by a microporous polypropylene film (Celgard 2325) and a porous glass microfiber filters (Whatman GF/F). The charge and discharge cycling tests (CELL TEST) were conducted in galvanostatic mode on an ATLAS 0961 MBI multichannel testing system within the operating voltage range of 3.0 ÷ 4.5 V with a current density of 0.1 and 0.2 C rate, at room temperature. The cyclic voltammetry (CV), as well as potentiostatic electrochemical impedance spectroscopy (EIS), were performed on a potentiostat/galvanostat AUTOLAB PGSTAT302N/FRA2. The CV scans were carried out at a scan rate of 0.1 mVs^{-1} from 3.0 to 4.5 V, starting from an open circuit potential (OCP). The EIS measurements were made with 0.1 V amplitude of an alternative current signal in the frequency range between 100 kHz and 0.1 Hz. The analysis of the data obtained during an electrochemical impedance measurements has been performed by fitting the experimental data with an equivalent circuit, based on the Boukamp model using Nova 1.8 Autolab software.

3. Results and Discussion

Fig. 1 shows the X-ray diffraction patterns of the prepared $LiMn_2O_{4-y}S_y$ materials. The diffraction peaks for the samples calcined at 300 °C (Fig. 1a) are broad and of low intensity, typical for defected spinels obtained at low

temperatures. Additional calcination at 650 °C (Fig. 1b) provides much better crystallized samples, with narrower and more intensive XRD peaks.

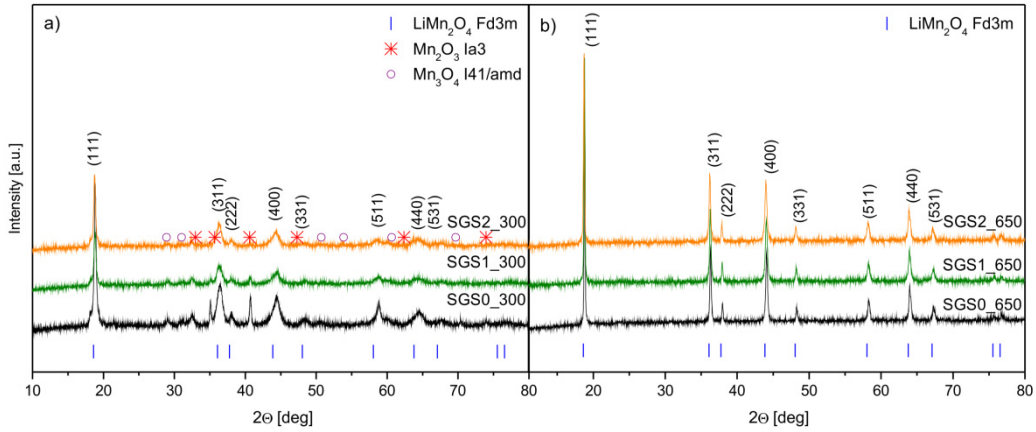

Fig. 1. XRD patterns of $LiMn_2O_{4-y}S_y$ spinels calcined at 300 °C (a) and at 650 °C (b).

For the low-temperature samples, the best fit of XRD patterns was achieved using three phase system: $LiMn_2O_4$ spinel (ICDD no. 00-035-0782), hausmannite Mn_3O_4 (ICDD no. 00-024-0734) and bixbyite Mn_2O_3 (ICDD no. 00-041-1442), whereas samples calcinated at 650 °C were identified as a single phase of cubic $LiMn_2O_4$ spinel structure with Fd3m space group, in which the lithium ions occupy the tetrahedral (8a) sites and the manganese ions occupy octahedral (16d) positions. The lattice constant of the synthesized materials was calculated by the Rietveld refinement using the XRD data and listed in Table 1. The lattice constants for SGS1 and SGS2 samples are slightly increased with increase in sulphur content what confirms sulphur substitution for oxygen in the spinel structure. The average crystallites size of the Li-Mn-O-S powders calculated by Scherrer formula is in a range from 21 to 48 nm (Table 1).

Table 1. Chemical composition, lattice constant, average crystallites size and electrical properties of the synthesized $LiMn_2O_{4-y}S_y$ spinels.

Sample	Nominal composition	Lattice constant (nm)	Average crystallites size (nm)	Electrical conductivity at ~25 °C (10^{-5} Scm^{-1})	Activation energy (eV)
SGS0_300	$LiMn_2O_4$	0.8159	22	1.21	0.29
SGS0_650	$LiMn_2O_4$	0.8171	48	5.10	0.38
SGS1_300	$LiMn_2O_{3.99}S_{0.01}$	0.8171	21	1.51	0.31
SGS1_650	$LiMn_2O_{3.99}S_{0.01}$	0.8182	47	6.30	0.37
SGS2_300	$LiMn_2O_{3.98}S_{0.02}$	0.8195	23	2.27	0.32
SGS2_650	$LiMn_2O_{3.98}S_{0.02}$	0.8211	48	9.79	0.40

In Fig. 2 the results of DSC measurements of the obtained spinels calcined at 650 °C are presented. The heat effects observed during heating and cooling for SGS0_650 sample are related to the first order phase transition of the spinel from cubic to orthorhombic structure. These effects for the sulphided Li-Mn-O-S spinels are strongly diminished. Therefore, it may be concluded that the partial deformation of the MnO_6 octahedra resulting from the substitution of oxygen with sulphur stabilizes the spinel structure and suppresses the phase transition.

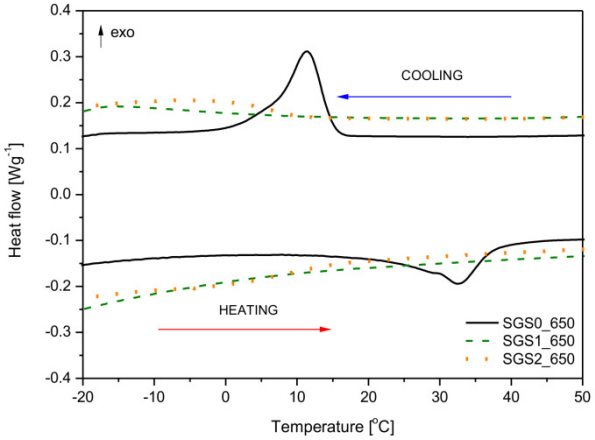

Fig. 2. DSC curves of the spinel materials calcined at 650 °C.

The temperature dependence of conductivity for the spinels is shown in Fig. 3. The obtained results are in good accordance with DSC outcomes.

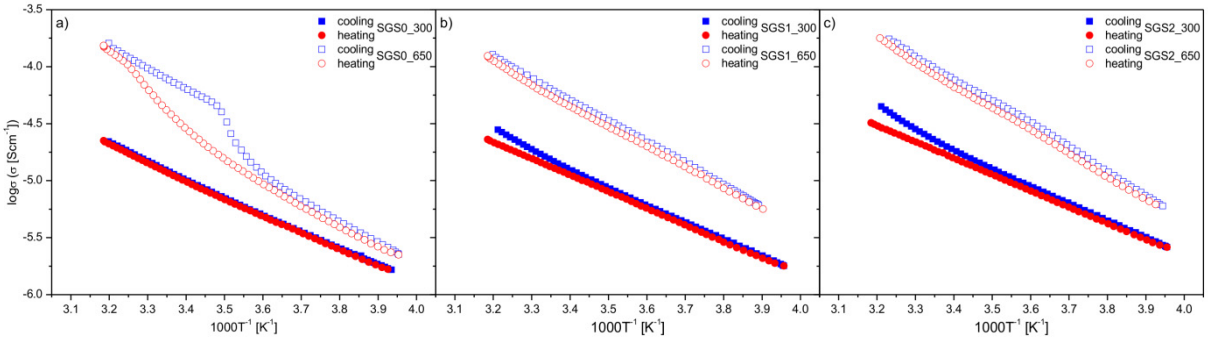

Fig.3. Electrical conductivity of SGS0 (a), SGS1 (b) and SGS2 (c) samples.

The observed nonlinearity of the electrical characteristics of SGS0_650 sample (Fig. 3a) is related to the phase transition. Nevertheless, with increase of sulphur content, this effect is suppressed (Fig. 3b and 3c). In Table 1 the values of electrical conductivity at around 25 °C and the activation energy in the -20 to 40 °C temperature range are presented. One can see that spinels calcined at 300 °C reveal low electrical conductivity. Calcination at 650 °C improved the σ value though the activation energy is increased.

Fig. 4 shows the initial charge and discharge curves of the Li/Li$^+$/$LiMn_2O_{4-y}S_y$ cells at 0.1C (Fig. 4a) and 0.2C (Fig. 4b) current rate between 3.0 and 4.5 V at room temperature.

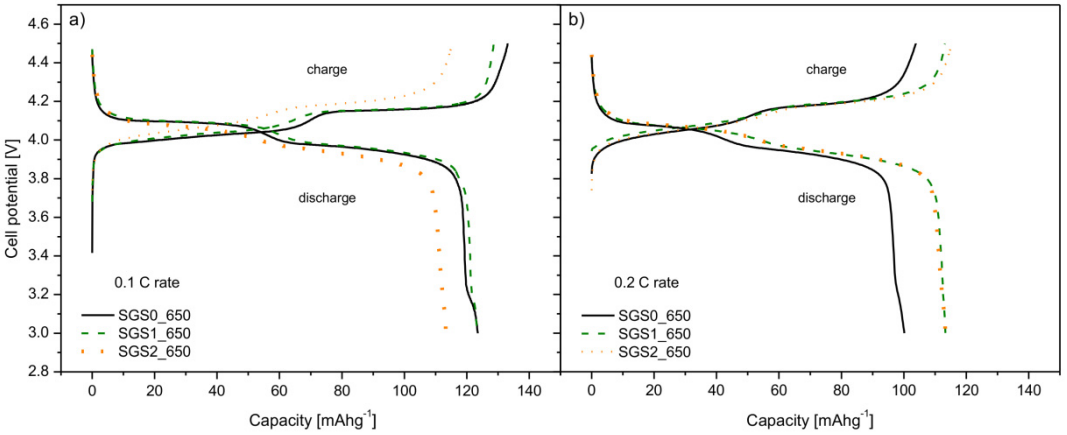

Fig. 4. Initial charge-discharge curves of sulphur doped lithium manganese spinels at 0.1 (a) and 0.2 (b) current rate.

All cells exhibit two potential plateau at around 4.0 and 4.15 V for the charge and discharge profiles which is characteristic of the $LiMn_2O_4$ spinel. The charge and discharge capacity of the lithium-ion batteries as a function of the number of cycles is depicted in Fig. 5.

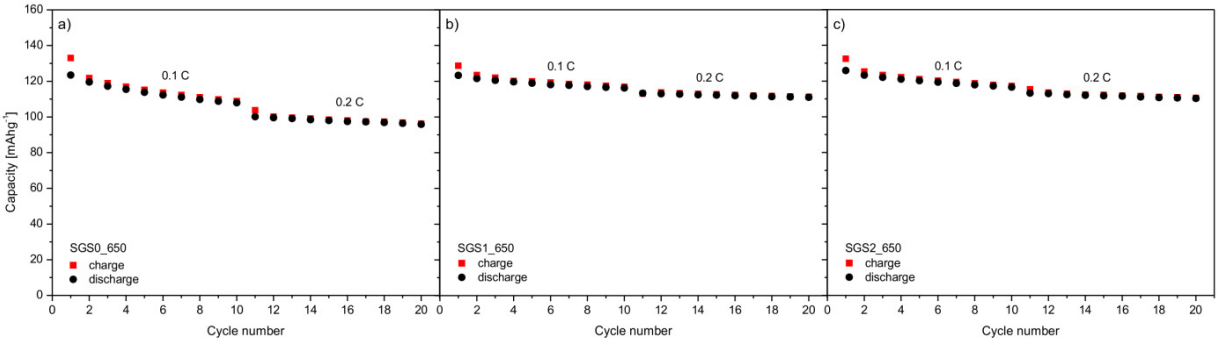

Fig. 5. Specific charge-discharge capacities versus cycle number for SGS0_650 (a), SGS1_650 (b) and SGS2_650 (c) cathode materials at different current rates.

In general, all electrodes exhibit high initial charge and discharge capacity. However, Li-Mn-O-S systems show better cyclability and rate capability. As shown, the lithium cells with sulphur doped spinel as the cathode active material (Fig. 5b and 5c) have better performance than SGS0_650 electrode (Fig. 5a). The $LiMn_2O_4$ electrode has an initial charge capacity of 133 and 104 $mAhg^{-1}$, with retention of 82% and 92% after 10 cycles at 0.1C and 0.2C current rate respectively. By contrast the charge capacity of sulphided spinels at a current rate of 0.1C and 0.2C is 129 and 113 $mAhg^{-1}$ for SGS1_650 and 133 and 115 $mAhg^{-1}$ for SGS2_650 sample. Moreover, about 88 to 98% of these capacities are retained after 10 cycles. This indicates that the sulphur substitution in the spinel structure improves the electrochemical performance of the $LiMn_2O_4$ spinel. It is worth to notice that smaller capacity fading is observed for higher working currents and that both cells containing oxysulphided spinels revealed very good columbic efficiency.

Five subsequent cyclic voltammogram curves of nonstoichiometric SGS1_650 (b) and SGS2_650 (c) electrode, measured at room temperature in the range of 3.0 ÷ 4.5 V with 0.1 mVs^{-1} scan rate are presented in Fig. 6. These CV curves are very typical for stoichiometric SGS0_650 electrode (Fig. 6a) that indicates two pairs of reversible oxidation and reduction current peaks at 4.2, 4.35 V and 3.8, 3.95 V respectively, corresponding to the two plateaus

in the charge/discharge profiles in Fig. 4. It is known that these CV curves are characterized by a well reversible two-step process during Li^+ intercalation and deintercalation which is typical of the Li-Mn-O system ($LiMn_2O_4 \leftrightarrow Li_{0.5}Mn_2O_4 \leftrightarrow \lambda$-$MnO_2$). Besides the two-well defined and well-known redox peaks, a peak at around 3.6 V is observed for SGS0_650 sample in the 5th cycle. It may be related to the formation of Li_2MnO_3 impurities during cycle due to the disproportionate reaction.

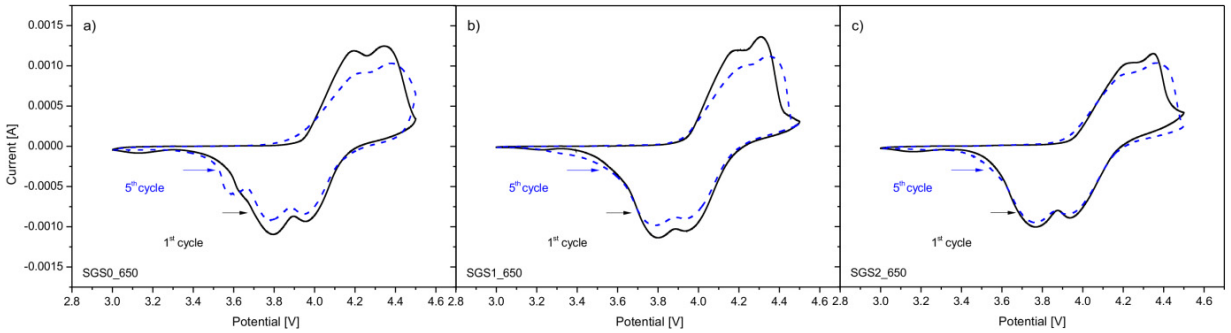

Fig. 6. Cyclic voltammetric curves for stoichiometric SGS0_650 (a) and nonstoichiometric SGS1_650 (b) and SGS2_650 (c) Li-Mn-O-S electrodes with scan rate of 0.1 mVs^{-1}.

The ac impedance spectra of $Li/Li^+/LiMn_2O_{4-y}S_y$ cells are shown in Fig. 7. The Nyquist plots are represented by a semicircle in the high and medium frequency range and a straight line at low frequencies.

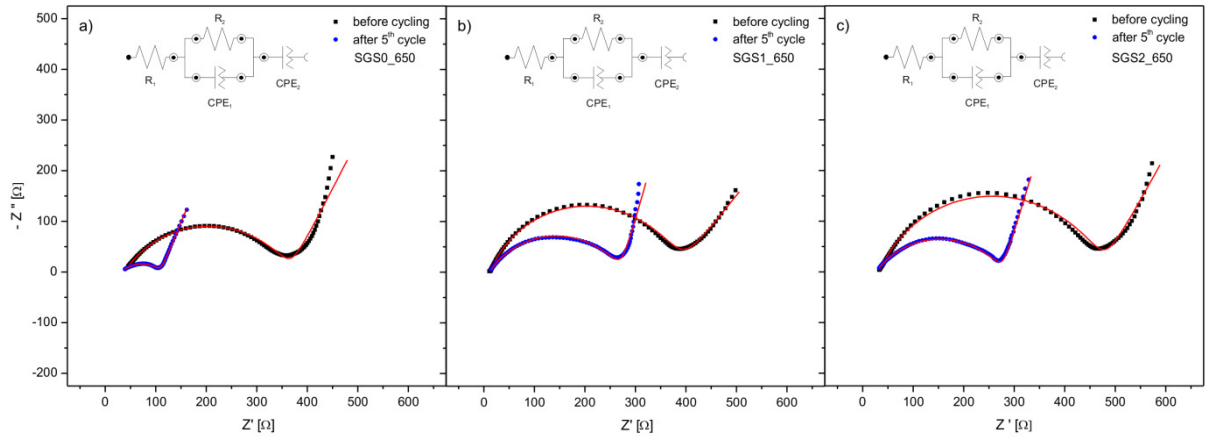

Fig. 7. Nyquist plots for $Li/Li^+/LiMn_2O_4$ (a), $Li/Li^+/LiMn_2O_{3.99}S_{0.01}$ (b) and $Li/Li^+/LiMn_2O_{3.98}S_{0.02}$ (c) cells and equivalent circuit used for the EIS fitting.

The electrochemical impedance spectra can be explained on the basis of the proposed equivalent circuit (Fig. 7), the same for all cells. In this circuit, R_1 is attributed to the uncompensated resistance and corresponds to the high frequency intercept at the real axis. The uncompensated resistance is the resistance between the electrode and the current-collector. A parallel sub-circuit comprising a resistor R_2 (a charge-transfer resistance), and a constant phase angle element CPE_1 (closely related to the electric double layer capacitor) is used to simulate the semicircle. The diameter of the semicircle corresponds to the charge-transfer resistance (R_2), which is related to the electrochemical reaction at the electrode/electrolyte interface and particle-particle contact. A large semicircle means a high charge-transfer resistance. In addition, another CPE element (CPE_2) is used in the equivalent circuit to stimulate the low-frequency straight line. This is actually a Warburg-type impedance, which is associated with Li ion diffusion in the

bulk of the active material at very low frequency. Calculated values of each resistor from the fitted equivalent circuits are collected in Table 2.

Table 2. Parameters of EIS measurements - calculated values of resistors in proposed equivalent circuits.

	R_1 (Ω)	R_2 (Ω)
$Li/Li^+/LiMn_2O_4$		
Before cycling	38	329
After 5th cycle	33	78
$Li/Li^+/LiMn_2O_{3.99}S_{0.01}$		
Before cycling	12	372
After 5th cycle	11	262
$Li/Li^+/LiMn_2O_{3.98}S_{0.02}$		
Before cycling	33	442
After 5th cycle	27	252

A decrease of R_2 values after five cycles for all spinel cathode materials is a direct indication of the formation of lithium easy diffusion paths as well as faster charge-transfer between the $LiMn_2O_{4-y}S_y$ nanoparticles. The χ^2 values in this study were about 10^{-2} and the estimated errors of the calculated parameters were less than 4%.

4. Conclusions

Sulphur doped lithium manganese spinels have been successfully synthesized by the modified sol-gel process. Based on this method, nanostructured materials with different sulphur content were obtained. Due to the introduction of a small amount of sulphur in the $LiMn_2O_4$ spinel structure, the unfavorable phase transition at around room temperature was diminished. The electrical conductivity measurements as well as electrochemical tests proved that prepared $LiMn_2O_{4-y}S_y$ spinels provide good electrochemical properties. The obtained materials exhibit high initial capacity, very good cyclability and reversibility. It was shown that sulphur doped lithium manganese spinel electrodes have better capacity than stoichiometric $LiMn_2O_4$. It is even more evident for higher current rate (0.2 C). Performed studies enabled optimization of sulphur content in the spinel structure. It was established that small amount of S (y = 0.01) in $LiMn_2O_{4-y}S_y$ does not deteriorate electrical conductivity of spinel and significantly improves its electrochemical performance, especially rate capability. The described properties bring excellent prospect in application of these systems as next generation cathode materials for Li-Ion batteries.

Acknowledgements

This work was supported by the European Institute of Innovation and Technology under the KIC InnoEnergy NewMat project.

References

[1] Y. Chen, K. Xie, Y. Pan, C. Zheng, Nano-sized $LiMn_2O_4$ spinel cathode materials exhibiting high rate discharge capability for lithium ion batteries, J. Power Sources 196 (2011) 6493-6497.
[2] Y.J. Hong, M.Y. Son, J-K. Lee, H.B. Lee, S.H. Lee, Y.C. Kang, Characteristics of stabilized spinel cathode powders obtained by in-situ coating method, J. Power Sources 244 (2013) 625-630.
[3] Z. Yang, Y. Jiang, H-H. Xu, Y-H. Huang, High-performance porous nanoscaled $LiMn_2O_4$ prepared by a polymer-assisted sol-gel method, Electrochim. Acta 106 (2013) 63-68.
[4] J.M. Tarascon, M. Armand, Issues and challenges facing rechargeable lithium batteries, Nature 414 (2001) 359-367.
[5] B. Scrosati, J. Garche, Lithium batteries: Status, prospects and future, J. Power Sources 195 (2010) 2419-2430.
[6] J.W. Fergus, Recent developments in cathode materials for lithium ion batteries, J. Power Sources 195 (2010) 939-954.
[7] E. Iwata, K. Takahashi, K. Maeda, T. Mouri, Capacity failure on cycling or storage of lithium-ion batteries with Li–Mn–O ternary phases having spinel-framework structure and its possible solution, J. Power Sources 81-82 (1999) 430-433.
[8] L. Yang, M. Takahashi, B. Wang, A study on capacity fading of lithium-ion battery with manganese spinel positive electrode during cycling, Electrochim. Acta 51 (2006) 3228-3234.
[9] A.R. Naghash, J.Y. Lee, Effect of oxygen non-stoichiometry on the electrochemical performance of lithium manganese oxide spinels, J. Power Sources 102 (2001) 68-73.

[10] L. Hernán, J. Morales, L. Sánchez, E. Rodríguez Castellón, M.A.G. Aranda, Synthesis, characterization and comparative study of the electrochemical properties of doped lithium manganese spinels as cathodes for high voltage lithium batteries, J. Mater. Chem. 12 (2002) 734-741.
[11] M. Hibino, M. Nakamura, Y. Kamitaka, N. Ozawa, T. Yao, Improvement of cycle life of spinel type of lithium manganese oxide by addition of other spinel compounds during synthesis, Solid State Ionics 177 (2006) 2653-2656.
[12] Y.J. Hong, M.Y. Son, J-K. Lee, H.B. Lee, S.H. Lee, Y.C. Kang, Characteristics of stabilized spinel cathode powders obtained by in-situ coating method, J. Power Sources 244 (2013) 625-630.
[13] M. Molenda, R. Dziembaj, D. Majda, M. Dudek, Synthesis and characterization of sulfied lithium manganese spinels $LiMn_2O_{4-y}S_y$ prepared by sol-gel method, Solid State Ionics 176 (2005) 1705-1709.
[14] M. Molenda, R. Dziembaj, E. Podstawka, W. Łasocha, L.M. Proniewicz, Influence of sulphur substitution on structural and electrical properties of lithium-manganese spinels, J. Phys. Chem. Solids 67 (2006) 1347-1350.
[15] R. Dziembaj, M. Molenda, D. Majda, S. Walas, Synthesis, thermal and electrical properties of $Li_{1+\delta}Mn_{2-\delta}O_4$ prepared by a sol–gel method, Solid State Ionics 157 (2003) 81-87.